

ActionFormer: Localizing Moments of Actions with Transformers

Chenlin Zhang[†]

Nanjing University

zhangcl@lamda.nju.edu.cn

Jianxin Wu

Nanjing University

wujx2001@nju.edu.cn

Yin Li

University of Wisconsin-Madison

yin.li@wisc.edu

Abstract

Self-attention based Transformer models have demonstrated impressive results for image classification and object detection, and more recently for video understanding. Inspired by this success, we investigate the application of Transformer networks for temporal action localization in videos. To this end, we present ActionFormer—a simple yet powerful model to identify actions in time and recognize their categories in a single shot, without using action proposals or relying on pre-defined anchor windows. ActionFormer combines a multiscale feature representation with local self-attention, and uses a light-weighted decoder to classify every moment in time and estimate the corresponding action boundaries. We show that this orchestrated design results in major improvements upon prior works. Without bells and whistles, ActionFormer achieves 65.6% mAP at $tIoU=0.5$ on THUMOS14, outperforming the best prior model by 8.7 absolute percentage points and crossing the 60% mAP for the first time. Further, ActionFormer demonstrates strong results on ActivityNet 1.3 (36.0% average mAP) and the more recent EPIC-Kitchens 100 (+13.5% average mAP over prior works). Our code is available at https://github.com/happyharrycn/actionformer_release.

1. Introduction

Identifying action instances in time and recognizing their categories, known as temporal action localization (TAL), remains a challenging problem in video understanding. Significant progress has been made in developing deep models for TAL. Most previous works have considered using action proposals [36] or anchor windows [50], and developed convolutional [55, 85], recurrent [7], and graph [4, 76] neural networks for TAL. Despite a steady progress on major benchmarks, the accuracy of existing methods usually comes at a price of modeling complexity, with increasingly sophisticated proposal generation, anchor design, loss function,

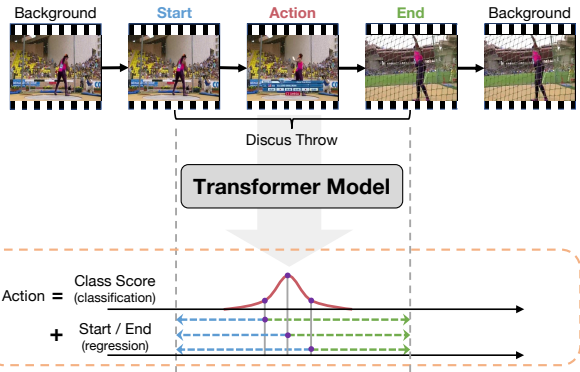


Figure 1. **An illustration of our ActionFormer.** We propose a Transformer based model to localize action instances in time (top) by (1) classifying every moment into action categories and (2) estimating their distances to action boundaries (bottom).

network architecture, and output decoding process.

In this paper, we adopt a minimalist design and develop a Transformer based model for TAL, inspired by the recent success of Transformers in NLP [19, 64] and vision [11, 20, 48]. Originally developed for sequence data, Transformers use self-attention to model long-range dependencies, and thus are a natural fit for TAL in untrimmed videos. Our method, illustrated in Fig. 1, adapts local self-attention to model temporal context in untrimmed videos, classifies every moment in an input video, and regresses their corresponding action boundaries. The result is a deep model that is trained using standard classification and regression loss, and can localize moments of actions in a single shot, without using action proposals or pre-defined anchor windows.

Specifically, our model, dubbed ActionFormer, integrates local self-attention to extract a feature pyramid from an input video. Each location in the output pyramid represents a moment in the video, and is treated as an action candidate. A lightweight convolutional decoder is further employed on the feature pyramid to classify these candidates into foreground action categories, and to regress the distance between a foreground candidate and its action onset and offset. The results can be easily decoded into actions with their labels and temporal boundaries. Our method thus provides a *single-stage anchor-free* model for TAL.

[†] Work was done when visiting UW Madison.

We show that such a simple model, with proper design, can be surprisingly powerful for TAL. In particular, ActionFormer establishes a new state of the art across several major TAL benchmarks, surpassing previous works by a significant margin. For example, ActionFormer achieves 65.6% *mAP* at $tIoU=0.5$ on THUMOS14, outperforming the best prior model by 8.7 absolute percentage points and crossing the 60% *mAP* for the first time. Further, ActionFormer reaches an average *mAP* of 36.0% on ActivityNet 1.3, and shows impressive results on EPIC-Kitchens 100 with an increase of over 13.5 absolute percentage points in average *mAP*.

Our work is based on simple techniques, supported by favourable empirical results, and validated by extensive ablation experiments, at our best. Our main contributions are summarized into three folds. First, we are among the first to propose a Transformer based model for single-stage anchor-free TAL. Second, we study key design choices of developing Transformer models for TAL, and demonstrate a simple model that works surprisingly well. Finally, our model achieves state-of-the-art results across major TAL benchmarks and offers a solid baseline for the field.

2. Related Works

We review previous works on TAL including two-stage and single-stage models, and briefly cover related works on action detection, object detection, and vision Transformers.

Two-stage TAL. A two-stage approach for TAL first generates candidate video segments as action proposals, and further classify the proposals into action categories and refine their temporal boundaries. Several previous works focused on action proposal generation, by either classifying anchor windows [8, 9, 22] or detecting action boundaries [26, 36, 38, 47, 84], and more recently using a graph representation [4, 76] or Transformers [13, 59, 67]. Others have integrated proposal generation and classification into a single model [14, 55, 56, 85]. More recent effort investigates the modeling of temporal context among proposals using graph neural networks [76, 80, 83] or attention and self-attention mechanisms [51, 58, 88]. Similar to previous approaches, our method considers the modeling of long-term temporal context, yet uses a self-attention within a Transformer model. Different from previous approaches, our model can detect actions in a single pass and without using proposals.

Single-stage TAL. There are a few recent works on single-stage TAL, seeking to localize actions in a single shot without using action proposals. Many of these methods are anchor-based (*e.g.*, using anchor windows sampled from sliding windows). For example, Lin *et al.* [37] presented the first single-stage TAL using convolutional networks, borrowing ideas from a single-stage object detector [44]. Buch *et al.* [7] presented a recurrent memory module for single-stage TAL. Long *et al.* [50] proposed to use Gaussian kernels to

dynamically optimize the scale of each anchor, based on a 1D convolutional network. Yang *et al.* [78] explored the combination of anchor-based and anchor-free models for single-stage TAL, again using convolutional networks. More recently, Lin *et al.* [35] proposed an anchor-free single-stage model by designing a saliency-based refinement module incorporated in convolutional network. Anchor-free temporal localization [81] has been explored in video grounding.

Our model falls into the category of single-stage TAL. Indeed, our formulation follows a minimalist design of sequence labeling by classifying every moment and regressing their action boundaries, previously discussed in [35, 78]. The key difference is that we design a Transformer network for action localization, while all previous methods used convolutional networks. The result is a single stage anchor-free model that outperforms all previous methods. A concurrent work from Liu *et al.* [46] also considered Transformer for TAL, yet formulated the problem as set prediction similar to DETR [11]. We compare to [46] in our experiments.

Spatio-temporal Action Localization. A related yet different task, known as spatial-temporal action localization, is to detect the actions both temporally and spatially, in the form of moving bounding boxes of an actor. It is possible that TAL might be used as a first step for spatial-temporal localization. Notably, Girdhar *et al.* [25] proposed to use Transformer for spatial-temporal action localization. While both our work and [25] use Transformer, the two models differ significantly. We consider a sequence of video frames as the inputs, while [25] used a set of 2D object proposals. Moreover, our work addresses a different task of TAL.

Object Detection. TAL models have been heavily influenced by the developments of object detection models. Some of our model design, including the multiscale feature representation and convolutional decoder, is inspired by feature pyramid network [39] and RetinaNet [40]. Our training using center sampling also stems from recent single-stage object detectors [21, 60, 82].

Vision Transformer. Transformer models were originally developed for NLP tasks [64], and has demonstrated recent success for many vision tasks. ViT [20] presented the first pure Transformer-based model that can achieve state-of-the-art performances on image classification. Subsequent works, including DeiT [61], T2T-ViT [79], Swin Transformer [48], Focal Transformer [77] and PVT [70], have further pushed the envelope, resulting in vision Transformer backbones that are accurate and efficient for classification, segmentation, and detection tasks. Transformer have also been explored in object detection [11, 17, 69, 87], semantic segmentation [15, 71, 73], and more recently video representation learning [3, 23, 49]. Our model builds on these developments and presents one of the first Transformer models for TAL.

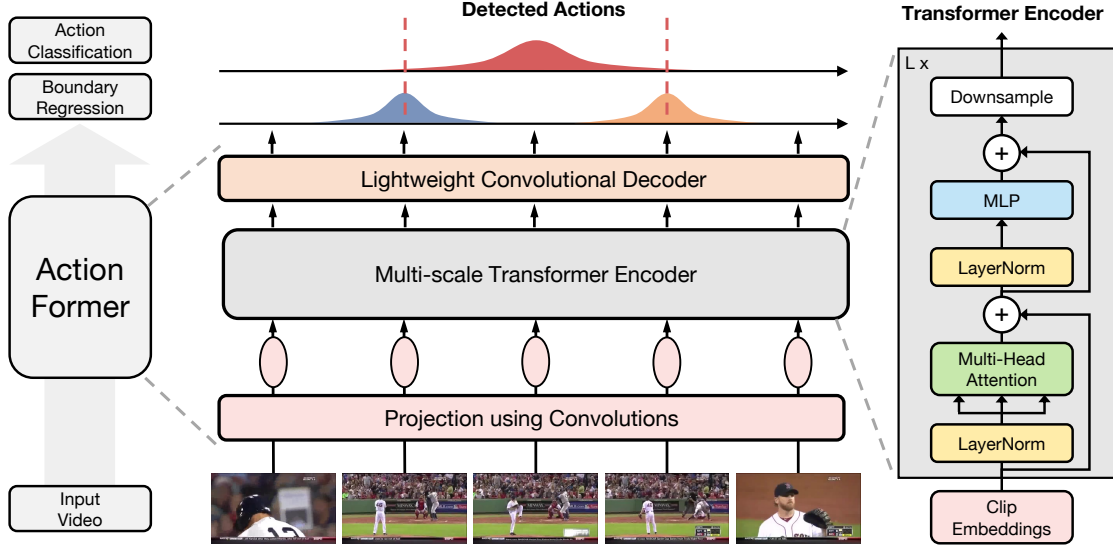


Figure 2. Overview of our ActionFormer. Our method builds a Transformer based model to detect an action instance by classifying every moment and estimating action boundaries. Specifically, ActionFormer first extracts a sequence of video clip features, and embeds each of these features. The embedded features are further encoded into a feature pyramid using a multi-scale transformer (right). The feature pyramid is then examined by shared classification and regression heads, producing an action candidate at every time step. Our method provides a single-stage anchor-free model for temporal action localization with strong performance across several datasets.

3. ActionFormer: A Simple Transformer Model for Temporal Action Localization

Given an input video \mathbf{X} , we assume that \mathbf{X} can be represented using a set of feature vectors $\mathbf{X} = \{\mathbf{x}_1, \mathbf{x}_2, \dots, \mathbf{x}_T\}$ defined on discretized time steps $t = \{1, 2, \dots, T\}$, where T varies across videos. For example, \mathbf{x}_t can be the feature vector of a clip at moment t extracted from a 3D convolutional network. The goal of temporal action localization is to predict the action label $\mathbf{Y} = \{\mathbf{y}_1, \mathbf{y}_2, \dots, \mathbf{y}_N\}$ based on the input video sequence \mathbf{X} . \mathbf{Y} consists of N action instances \mathbf{y}_i , where N also varies across videos. Each instance $\mathbf{y}_i = (s_i, e_i, a_i)$ is defined by its starting time s_i (onset), ending time e_i (offset) and its action label a_i , where $s_i \in [1, T]$, $e_i \in [1, T]$, $a_i \in \{1, \dots, C\}$ (C pre-defined categories) and $s_i < e_i$. The task of TAL is thus a challenging structured output prediction problem.

A Simple Representation for Action Localization. Our method builds on an anchor-free representation for action localization, also described in [35, 78]. The key idea is to classify each moment as either one of the action categories or the background, and further regress the distance between this time step and the action’s onset and offset. In doing so, we convert the structured output prediction problem ($\mathbf{X} = \{\mathbf{x}_1, \mathbf{x}_2, \dots, \mathbf{x}_T\} \rightarrow \mathbf{Y} = \{\mathbf{y}_1, \mathbf{y}_2, \dots, \mathbf{y}_N\}$) into a more approachable sequence labeling problem

$$\mathbf{X} = \{\mathbf{x}_1, \mathbf{x}_2, \dots, \mathbf{x}_T\} \rightarrow \hat{\mathbf{Y}} = \{\hat{\mathbf{y}}_1, \hat{\mathbf{y}}_2, \dots, \hat{\mathbf{y}}_T\}. \quad (1)$$

The output $\hat{\mathbf{y}}_t = (p(a_t), d_t^s, d_t^e)$ at time t is defined as

- $p(a_t)$ consists of C values, with each representing a

binomial variable indicating the probability of action category a_t ($\in \{1, 2, \dots, C\}$) at time t . This can be considered as the outputs of C binary classification.

- $d_t^s > 0$ and $d_t^e > 0$ are the distance between the current time t to the action’s onset and offset, respectively. d_t^s and d_t^e are not defined if time t lies on the background.

Intuitively, this formulation considers *every moment* t in the video \mathbf{X} as an action candidate, recognizes the action’s category a_t , and estimates the distances between current step and the action boundaries (d_t^s and d_t^e) if an action presents. Action localization results can be readily decoded from $\hat{\mathbf{y}}_t = (p(a_t), d_t^s, d_t^e)$ by

$$a_t = \arg \max p(a_t), \quad s_t = t - d_t^s, \quad e_t = t + d_t^e. \quad (2)$$

Method Overview. Our model — ActionFormer learns to label an input video sequence $f(\mathbf{X}) \rightarrow \hat{\mathbf{Y}}$. Specifically, f is realized using a deep model. ActionFormer follows an encoder-decoder architecture proven successful in many vision tasks, and decomposes f as $h \circ g$. Here $g: \mathbf{X} \rightarrow \mathbf{Z}$ encodes the input into a latent vector \mathbf{Z} , and $h: \mathbf{Z} \rightarrow \hat{\mathbf{Y}}$ subsequently decodes \mathbf{Z} into the sequence label $\hat{\mathbf{Y}}$.

Fig. 2 presents an overview of our model. Importantly, our encoder g is parameterized by a Transformer network [64]. Our decoder h adopts a lightweight convolutional network. To capture actions at disparate temporal scales, we design a multi-scale feature representation $\mathbf{Z} = \{\mathbf{Z}^1, \mathbf{Z}^2, \dots, \mathbf{Z}^L\}$ forming a feature pyramid with varying resolutions. We now describe the details of our model.

3.1. Encode Videos with Transformer

Our model first encodes an input video $\mathbf{X} = \{\mathbf{x}_1, \mathbf{x}_2, \dots, \mathbf{x}_T\}$ into a multiscale feature representation $\mathbf{Z} = \{\mathbf{Z}^1, \mathbf{Z}^2, \dots, \mathbf{Z}^L\}$ using an encoder g . The encoder g consists of (1) a projection function using a convolutional network that embeds each feature (\mathbf{x}_t) into a D -dimensional space; and (2) a Transformer network that maps the embedded features to the output feature pyramid \mathbf{Z} .

Projection. Our projection \mathbf{E} is a shallow convolutional network with ReLU as the activation function, defined as

$$\mathbf{Z}^0 = [\mathbf{E}(\mathbf{x}_1), \mathbf{E}(\mathbf{x}_2), \dots, \mathbf{E}(\mathbf{x}_T)]^T, \quad (3)$$

where $\mathbf{E}(\mathbf{x}_i) \in \mathbb{R}^D$ is the embedded feature of \mathbf{x}_i . Adding convolutions before a Transformer network was recently found helpful to better incorporate local context for time series data [32] and to stabilize the training of vision Transformers [72]. An position embeddings [64] $\mathbf{E}_{pos} \in \mathbb{R}^{T \times D}$ can be optionally added. Yet we find that doing so will decrease the performance of the model, and have thus removed position embeddings in our model by default.

Self-Attention. The Transformer network further takes \mathbf{Z}^0 as input. The core of a Transformer is self-attention [64]. We briefly introduce the key idea here. Concretely, self-attention computes a weighted average of features with the weight proportional to a similarity score between pairs of input features. For example, given $\mathbf{Z}^0 \in \mathbb{R}^{T \times D}$ with T time steps of D dimensional features, \mathbf{Z}^0 is projected using $\mathbf{W}_Q \in \mathbb{R}^{D \times D_q}$, $\mathbf{W}_K \in \mathbb{R}^{D \times D_k}$, and $\mathbf{W}_V \in \mathbb{R}^{D \times D_v}$ to extract feature representations \mathbf{Q} , \mathbf{K} , and \mathbf{V} , referred to as query, key and value respectively with $D_k = D_q$. The outputs \mathbf{Q} , \mathbf{K} , \mathbf{V} are computed as

$$\mathbf{Q} = \mathbf{Z}^0 \mathbf{W}_Q, \quad \mathbf{K} = \mathbf{Z}^0 \mathbf{W}_K, \quad \mathbf{V} = \mathbf{Z}^0 \mathbf{W}_V. \quad (4)$$

The output of self-attention is given by,

$$\mathbf{S} = \text{softmax} \left(\mathbf{Q} \mathbf{K}^T / \sqrt{D_q} \right) \mathbf{V}, \quad (5)$$

where $\mathbf{S} \in \mathbb{R}^{T \times D}$ and softmax is a *row-wise* softmax normalization function. A multiheaded self-attention (MSA) further adds several self-attention operations in parallel.

Local Self-Attention. A main advantage of MSA is the ability to integrate temporal context across the full sequence, yet such a benefit comes at the cost of computation. A vanilla MSA has a complexity of $O(T^2)$ in both memory and time, and is thus highly inefficient for long sequences. There has been several recent work on efficient self-attention [5, 16, 68, 74]. Here we adapt the local self-attention from [16] by limiting the attention within a local window. Our intuition is the temporal context beyond a certain range is less helpful for action localization. Note that the local self-attention is used together with the multiscale feature representation $\mathbf{Z} = \{\mathbf{Z}^1, \mathbf{Z}^2, \dots, \mathbf{Z}^L\}$. More precisely, the same window

size is applied to each feature level. Even a small window size (*e.g.* 19) on a downsampled feature map (*e.g.* 16x) will cover a large temporal range (304).

Multiscale Transformer. We now present the design of our Transformer encoder. Our Transformer has L Transformer layers with each layer consisting of alternating layers of local multiheaded self-attention (MSA) and MLP blocks. Moreover, LayerNorm (LN) is applied before every MSA or MLP block, and residual connection is added after every block. GELU is used for the MLP. To capture actions at different temporal scales, a downsampling operator $\downarrow(\cdot)$ is optionally attached. This is given by

$$\begin{aligned} \mathbf{Z}^\ell &= \alpha^\ell \text{MSA}(\text{LN}(\mathbf{Z}^{\ell-1})) + \mathbf{Z}^{\ell-1}, \quad \ell = 1 \dots L \\ \bar{\mathbf{Z}}^\ell &= \bar{\alpha}^\ell \text{MLP}(\text{LN}(\bar{\mathbf{Z}}^\ell)) + \bar{\mathbf{Z}}^\ell, \quad \ell = 1 \dots L \\ \hat{\mathbf{Z}}^\ell &= \downarrow(\bar{\mathbf{Z}}^\ell), \quad \ell = 1 \dots L, \end{aligned} \quad (6)$$

where $\mathbf{Z}^{\ell-1}, \bar{\mathbf{Z}}^\ell, \hat{\mathbf{Z}}^\ell \in \mathbb{R}^{T^{\ell-1} \times D}$ and $\mathbf{Z}^\ell \in \mathbb{R}^{T^\ell \times D}$. $T^{\ell-1}/T^\ell$ is the downsampling ratio. α^ℓ and $\bar{\alpha}^\ell$ are learnable per-channel scaling factors initialized to zeros as in [62].

The downsampling operator \downarrow is implemented using a single strided depthwise 1D convolution due to its efficiency. We use 2x downsampling for our model. Our Transformer block is shown in Fig. 2 (right). Our model combines several Transformer blocks with downsampling in between, resulting in a feature pyramid $\mathbf{Z} = \{\mathbf{Z}^1, \mathbf{Z}^2, \dots, \mathbf{Z}^L\}$.

3.2. Decoding Actions in Time

Next, our model decodes the feature pyramid \mathbf{Z} from the encoder g into the sequence label $\hat{\mathbf{Y}} = \{\hat{\mathbf{y}}_1, \hat{\mathbf{y}}_2, \dots, \hat{\mathbf{y}}_T\}$ using the decoder h . Our decoder is a lightweight convolutional network with a classification and a regression head.

Classification Head. Given the feature pyramid Z , our classification head examines each moment t across all L levels on the pyramid, and predicts the probability of action $p(a_t)$ at every moment t .² This head is realized using a lightweight 1D convolutional network attached to each pyramid level. And the parameters are shared across all levels. Our classification network is implemented using 3 layers of 1D convolutions with kernel size=3, layer normalization (for the first 2 layers), and ReLU activation. A sigmoid function is attached to each output dimension to predict the probability of C action categories. Adding layer normalization slightly boosts the performance as we will demonstrate in our ablation.

Regression Head. Similar to our classification head, our regression head examines every moment t across all L levels on the pyramid. The difference is that the regression head predicts the distances to the onset and offset of an action (d_t^s, d_t^e) , only if the current time step t lies in an action. An output regression range is pre-specified for each pyramid level. The regression head, again, is implemented using a

²Without loss of clarity, we drop the index of the pyramid ℓ .

1D convolutional network following the same design of the classification network, except that a ReLU is attached at the end for distance estimation.

3.3. Training and Inference

Loss Function. Our model outputs $(p(a_t), d_t^s, d_t^e)$ for every moment t , including the probability of action categories $p(a_t)$ and the distances to action boundaries (d_t^s, d_t^e) . Our loss function, again following minimalist design, only has two terms: (1) \mathcal{L}_{cls} a focal loss [40] for C way binary classification; and (2) \mathcal{L}_{reg} a generalized IoU loss [54] for distance regression. The loss is defined for each video X as

$$\mathcal{L} = \sum_t \left(\frac{1}{T} \mathcal{L}_{cls} + \frac{\lambda_{reg}}{T_+} \mathbb{1}_{c_t} \mathcal{L}_{reg} \right), \quad (7)$$

where T is the length of the input sequence. $\mathbb{1}_{c_t}$ is an indicator function that denotes if a time step t is within an action, *i.e.* a positive sample. T_+ is the total number of positive samples. \mathcal{L} is applied to all levels on the output pyramid, and averaged across all video samples during training. λ_{reg} is a coefficient that balances between the classification and regression loss. We set $\lambda_{reg} = 1$ by default and study the choice of λ_{reg} in our ablation.

Importantly, \mathcal{L}_{cls} considers uses focal loss [60] to recognize C action categories. Focal loss naturally handles imbalanced samples — there are much more negative samples than positive ones. Moreover, \mathcal{L}_{reg} adopts a differentiable IoU loss [54]. \mathcal{L}_{reg} is only enabled only when the current time step contains a positive sample.

Center Sampling. During training, we find it helpful to adapt a center sampling strategy similar to [60, 82], as we will show in our ablation study. Specifically, when determining the positive samples, only time steps within an interval around the center of an action are considered positive, where the duration of interval is proportional to the feature stride of the current pyramid level ℓ . More precisely, given an action centered at c , any time step $t \in [c - \alpha T/T^\ell, c + \alpha T/T^\ell]$ at the pyramid level ℓ is considered as positive, where $\alpha = 1.5$. Using center sampling does not impact model inference, yet produces higher scores around the center of an action moment, as shown in our ablation.

Design of the Feature Pyramid. A critical component of our model is the design of the temporal feature pyramid $\mathbf{Z} = \{\mathbf{Z}^1, \mathbf{Z}^2, \dots, \mathbf{Z}^L\}$. The design choices include (1) the number of levels within the pyramid; (2) the downsampling ratio between successive feature maps; and (3) the output regression range of each pyramid level. Inspired by the design of feature pyramid in modern object detectors (FPN [39] and FCOS [60]), we simplify our design choices by using a 2x downsampling of the feature maps, and roughly enlarging the output regression range by 2 accordingly. We will explore different design choices in our ablation.

Training Details. Following [25], we used Adam [31] with warm-up for training. The warm-up stage turned out to be critical for model convergence and to obtain good performance, as also pointed out by [42]. When training with variable length input, we fixed the maximum input sequence length, padded or cropped the input sequences accordingly, and added proper masking for all operations in the model. This is equivalent to training with sliding windows, as described in [78]. Varying the maximum input sequence length during training has little impact to the performance, as we will demonstrate in our ablation.

Inference. At inference time, we feed the full sequences into the model, as no position embeddings are used in the model. Our model takes the input video \mathbf{X} , and outputs $\{(p(a_t), d_t^s, d_t^e)\}$ for every time step t across all pyramid levels. Each time step t further decodes an action instance $(e_t = t - d_t^s, s_t = t + d_t^e, p(a_t))$. e_t and s_t are the onset and offset of the action, and $p(a_t)$ is an action confidence score. The result action candidates are further processed using Soft-NMS [6] to remove highly overlapping instances, leading to the final outputs of actions.

Network Architecture. We used 2 convolutions for projection, 7 Transformer blocks for the encoder (with 2x down-sampling for the last 5), and separate classification and regression heads as the decoder (each with 3 layers of 1D convolutions). The regression range on each pyramid level was normalized by the stride of the features. More implementation details are presented in the appendix.

4. Experiments and Results

We now present our experiments and results. Our main results include benchmarks on THUMOS14 [29], ActivityNet-1.3 [10] and EPIC-Kitchens 100 [18]. Moreover, we provide extensive ablation studies of our model.

Evaluation Metric. For all datasets, we report the standard mean average precision (mAP) at different temporal intersection over union (tIoU) thresholds, widely used to evaluate TAL methods. tIoU is defined as the intersection over union between two temporal windows, *i.e.* the 1D Jaccard index. Given a tIoU threshold (*e.g.*, 0.5), mAP computes the mean of average precision across all action categories. An average mAP is also reported by averaging across several tIoUs.

4.1. Results on THUMOS14

We start with our experiments and results on THUMOS14. We present the dataset, experiment setup, implementation details, our baselines and discuss the results.

Dataset. THUMOS14 [29] dataset contains 413 untrimmed videos with 20 categories of actions. The dataset is divided into two subsets: validation set and test set. The validation set contains 200 videos and the test set contains 213 videos.

Type	Model	Feature	THUMOS14						ActivityNet1.3			
			0.3	0.4	0.5	0.6	0.7	Avg.	0.5	0.75	0.95	Avg.
Two-Stage	CDC [55]	—	40.1	29.4	23.3	13.1	7.9	22.8	45.3	26.0	0.2	23.8
	BSN [38]	TSN [66]	53.5	45.0	36.9	28.4	20.0	36.8	46.5	30.0	8.0	30.0
	BMN [36]	TSN [66]	56.0	47.4	38.8	29.7	20.5	38.5	50.1	34.8	8.3	33.9
	DBG [34]	TSN [66]	57.8	49.4	39.8	30.2	21.7	39.8	—	—	—	—
	G-TAD [76]	TSN [66]	54.5	47.6	40.3	30.8	23.4	39.3	50.4	34.6	9.0	34.1
	G-TAD [76]+TSP [2]	R(2+1)D [63]	—	—	—	—	—	—	51.3	37.1	9.3	35.8
	TAL [14]	I3D [12]	53.2	48.5	42.8	33.8	20.8	39.8	38.2	18.3	1.3	20.2
	BC-GNN [4]	TSN [66]	57.1	49.1	40.4	31.2	23.1	40.2	50.6	34.8	9.4	34.3
	TAL-MR [84]	I3D [12]	53.9	50.7	45.4	38.0	28.5	43.3	43.5	33.9	9.2	30.2
	P-GCN [80]	I3D [12]	63.6	57.8	49.1	—	—	—	48.3	33.2	3.3	31.1
	P-GCN [80]+TSP [2]	R(2+1)D [63]	69.1	63.3	53.5	40.4	26.0	50.5	—	—	—	—
	C-TCN [33]	TSN [66]	68.0	62.3	52.1	—	—	—	47.6	31.9	6.2	31.1
	TSA-Net [26]	P3D [52]	61.2	55.9	46.9	36.1	25.2	45.1	48.7	32.0	9.0	31.9
	MUSES [45]	I3D [12]	68.9	64.0	56.9	<u>46.3</u>	31.0	—	50.0	35.0	6.6	34.0
	TCANet [51]	TSN [66]	60.6	53.2	44.6	36.8	26.7	44.3	52.3	36.7	6.9	35.5
	TCANet [51]	SlowFast [24]	—	—	—	—	—	—	54.3	39.1	8.4	37.6
	BMN-CSA [58]	TSN [66]	64.4	58.0	49.2	38.2	27.8	47.7	52.4	36.2	5.2	35.4
	ContextLoc [88]	I3D [12]	68.3	63.8	54.3	41.8	26.2	50.9	56.0	35.2	3.6	34.2
	VSGN [83]	TSN [66]	66.7	60.4	52.4	41.0	30.4	50.2	52.4	36.0	8.4	35.1
	VSGN [83]	I3D [12]	—	—	—	—	—	—	52.3	35.2	8.3	34.7
	VSGN [83]+TSP [2]	R(2+1)D [63]	—	—	—	—	—	—	53.3	<u>36.8</u>	8.1	35.9
	RTD-Net [59]	I3D [12]	68.3	62.3	51.9	38.8	23.7	49.0	47.2	30.7	8.6	30.8
Single-Stage	SSN [85]	TS [57]	51.0	41.0	29.8	—	—	—	43.2	28.7	5.6	28.3
	A ² Net [78]	I3D [12]	58.6	54.1	45.5	32.5	17.2	41.6	43.6	28.7	3.7	27.8
	GTAN [50]	P3D [52]	57.8	47.2	38.8	—	—	—	52.6	34.1	8.9	34.3
	PBRNet [43]	I3D [12]	58.5	54.6	51.3	41.8	29.5	—	54.0	35.0	9.0	35.0
	AFSD [35]	I3D [12]	67.3	62.4	55.5	43.7	<u>31.1</u>	52.0	52.4	35.3	6.5	34.4
	TadTR [46]	I3D [12]	62.4	57.4	49.2	37.8	26.3	46.6	49.1	32.6	8.5	32.3
	Ours	I3D [12]	75.5	72.5	65.6	56.6	42.7	62.6	53.5	36.2	8.2	35.6
	Ours+TSP [2]	R(2+1)D [63]	69.5	63.8	56.3	44.8	30.8	<u>53.1</u>	54.1	36.3	7.7	<u>36.0</u>

Table 1. **Results on THUMOS14 and ActivityNet1.3.** We report *mAP* at different tIoU thresholds. Average *mAP* in [0.3:0.1:0.7] is reported on THUMOS14 and [0.5:0.05:0.95] on ActivityNet1.3. Best results are in **bold** and second best underlined. Our method outperforms previous methods on THUMOS14 by a large margin, and beats previous methods when using the same features on ActivityNet1.3.

Follow the common practice [36, 38, 76, 84], we use the validation set for training and report results on the test set.

Experiment Setup & Implementation Details. We used two-stream I3D [12] pretrained on Kinetics to extract the video features on THUMOS14, following [41, 84]. We fed 16 consecutive frames as the input to I3D, used a sliding window with stride 4 and extracted 1024-D features before the last fully connected layer. The two-stream features were further concatenated (2048-D) as the input to our model. *mAP@[0.3:0.1:0.7]* was used to evaluate our model. Our model was trained for 50 epochs with a linear warmup of 5 epochs. The initial learning rate was 1e-4 and a cosine learning rate decay is used. The mini-batch size was 2, and a weight decay of 1e-4 was used. A window size of 19 was chosen for local self-attention based on our ablation. We also combined external classification scores from Untrimmed-Net [65] following previous works [4, 34, 76, 84]. We refer the readers to [80] (Appendix E) for a detailed description of the score fusion strategy.

To show that our method can adapt to different video features, we also consider the pre-training method from [2]

using an R(2+1)D network [63].

Baselines. We compare our method to a strong set of baselines, including both two-stage (*e.g.*, G-TAD [76], BC-GNN [4], TAL-MR [84]) and single-stage (*e.g.*, A2Net [78], GTAN [50], AFSD [35], TadTR [46]) methods for TAL. Our close competitors are those single-stage methods.

Despite our best attempt for a fair comparison to the baselines, we recognize some of our baselines used a different setup. For example, AFSD [35] took lower resolution input videos (96x96) when extracting I3D features. PBRNet [43] adopted a 2D feature map rather than a feature vector for each time step. A2Net [78] did not consider score fusion. Nonetheless, our experiment setup follows previous works [41, 84]. Our intent here is to compare our results to the best results previously reported.

Results. Table 1 (left) summarizes the results. Our method achieves an average *mAP* of 62.7% ([0.3 : 0.1 : 0.7]), with an *mAP* of 65.6% at tIoU=0.5 and an *mAP* of 42.6% at tIoU=0.7, outperforming all previous methods by a large margin (+8.7% *mAP* at tIoU=0.5 and +11.6% *mAP* at

tIoU=0.7). Our results stay on top of all single-stage methods, and also beats all previous two-stage methods, including the latest ones from [33, 51, 58, 84]. Note that our method significantly outperforms the concurrent work of TadTR [46], which also designed a Transformer model for TAL. With the combination of a simple design and a strong Transformer model, our method establishes new state of the art on THUMOS14, crossing the 60% average *mAP* at the first time.

4.2. Results on ActivityNet-1.3

Moving forward, we present our results on ActivityNet-1.3. Again, we introduce the dataset, describe our experiment setup, and discuss our results.

Dataset. ActivityNet-1.3 [10] is a large-scale action dataset which contains 200 activity classes and around 20,000 videos with more than 600 hours. The dataset is divided into three subsets: 10,024 videos for training, 4,926 for validation, and 5,044 for testing. Follow the common practice in [36, 38, 76], we train our model on the training set and report the performance on the validation set.

Experiment Setup & Implementation Details. We used two-stream I3D [12] for feature extraction, yet increased the stride of the sliding window to 16. Following [36, 38, 76], the extracted features were downsampled into a fixed length of 128 using linear interpolation. For evaluation, we used *mAP*@[0.5:0.05:0.95] and also reported the average *mAP*. Our model was trained for 15 epochs with a linear warmup of 5 epochs. The learning rate was 1e-3, the mini-batch size was 16, and the weight decay was 1e-4. A window size of 25 was used for local self-attention. Moreover, we combined external classification results from [86] following [4, 76, 80, 84]. Similarly, we consider the pre-training method from [2] and compare our model to the same set of baselines, including our close competitor of single-stage models.

Results. Table 1 (right) shows the results. With I3D features, our method reaches an average *mAP* of 35.6% ([0.5 : 0.05 : 0.95]), outperforming all previous methods using the same features by at least 0.6%. This boost is significant as the result is averaged across many tIoU thresholds, including those tight ones *e.g.* 0.95. Using the pre-training method from TSP [2] slightly improves our results (36.0% average *mAP*). Our model thus outperforms the best method with the same features [83] by a small margin. Again, our method largely outperforms TadTR [46]. Our results are only worse than TCA-Net [51] —a latest two-stage method using stronger SlowFast features [24]. We conjecture that our method will also benefit from better features. Nonetheless, our simple model clearly demonstrates state-of-the-art results on this challenging dataset.

4.3. Results on EPIC-Kitchens 100

Further, we conduct experiments on the newly released EPIC-Kitchens 100 [18] that has hundreds of instances from

Task	Method	0.1	0.2	0.3	0.4	0.5	Avg
Verb	BMN [18, 36]	10.8	9.8	8.4	7.1	5.6	8.4
	G-TAD [76]	12.1	11.0	9.4	8.1	6.5	9.4
	Ours	26.6	25.6	24.4	22.4	18.3	23.4
Noun	BMN [18, 36]	10.3	8.3	6.2	4.5	3.4	6.5
	G-TAD [76]	11.0	10.0	8.6	7.0	5.4	8.4
	Ours	25.5	24.3	22.6	20.3	16.6	21.9

Table 2. **Results on EPIC-Kitchens 100 validation set.** We report *mAP* at different tIoU thresholds and the average *mAP* in [0.1:0.1:0.5]. All methods used the same SlowFast features. Our method outperforms all baselines by a large margin.

different categories per video.

Dataset. EPIC-Kitchens 100 is the largest egocentric action dataset. The dataset contains 100 hours of videos from 700 sessions capturing cooking activities in different kitchens. In comparison to ActivityNet-1.3, EPIC-Kitchens 100 has less number of videos, yet many more instances per video (average 128 vs. 1.5 on ActivityNet-1.3). In comparison to THUMOS14, EPIC-Kitchens is 3 times larger in terms of video hours and more than 10 times larger in terms of action instances. This dataset is thus very challenging.

Experiment Setup & Implementation Details. We used a SlowFast network [24] pre-trained on EPIC-Kitchens for feature extraction. This model is provided by [18]. We fed 32 frame window with a stride of 16 to extract 2304-D features. Our model was trained on the training set and evaluated on the validation set. A window size of 19 was used for local self-attention. For evaluation, we used *mAP*@[0.1:0.1:0.5] and report the average *mAP* following [18]. In this dataset, an action is defined as a combination of a verb (action) and a noun (object). As this dataset was recently released, we are only able to compare our methods to BMN [36] and G-TAD [76], both using the same SlowFast features provided by [18]. Our model was trained for 30 epochs with learning rate 1e-4, mini-batch size 2, and weight decay of 1e-4.

Results. Table 2 presents the results. Our method achieves an average *mAP* ([0.1:0.1:0.5]) of 23.4% and 21.9% for verb and noun, respectively. Our results again largely outperform the strong baselines of BMN [36] and G-TAD [76] by over 13.5% in absolute percentage points. An interesting observation is that the gaps between our results and BMN / G-TAD are much larger on EPIC-Kitchens 100. BMN / G-TAD has an average *mAP* of 33.9% / 34.1% on ActivityNet-1.3, respectively. That is within 1.5% average *mAP* as our method. We conjecture that the difference might be attributed to the characteristics of the datasets. These results further confirm the effectiveness of our method.

4.4. Ablation Experiments

We conduct extensive ablation studies on THUMOS14 to understand our model design. The results are reported using I3D features with the same random seed for training.

Baseline: A Convolutional Network. Our ablation starts

Method	Backbone	LN	CTR	PE	Fusion	0.5	0.7	Avg
AF Base [78]	Conv					36.6	15.0	34.2
AF Base [35]	Conv					31.0	19.0	40.4
AF Base (Our Impl)	Conv					44.4	25.9	42.8
AF Base (Our Impl)	Conv				✓	55.0	33.1	53.1
Ours	Trans					61.4	36.1	58.7
Ours	Trans	✓				64.5	41.5	61.4
Ours	Trans	✓	✓			65.4	40.9	62.0
Ours	Trans	✓	✓	✓		65.3	40.7	61.6
Ours	Trans	✓	✓		✓	66.3	42.6	62.6
Ours (win size=19)	Trans	✓	✓		✓	65.6	42.7	62.6

Table 3. **Ablation study on model design.** We report *mAP* at $tIoU=0.5$ and 0.7 , and the average *mAP* in $[0.3 : 0.1 : 0.7]$ on THUMOS14. Our starting point is a baseline using a 1D convolutional network (AF Base). We gradually replace convolutions with our Transformer model, add layer norm to heads (LN), enable center sampling during training (CTR), explore position encoding (PE), and fuse classification scores (Fusion).

by re-implementing a baseline anchor-free method (AF Base) as described in [35, 78] (Table 3 row 1-2). This baseline shares the same action representation as our model, yet uses a 1D convolutional network as the encoder. We roughly match the number of layers and parameters of this baseline to our model. More details can be found in the appendix. This baseline, trained for 100 epochs, achieves an average *mAP* of 42.8% on THUMOS14 (Table 3 row 3), outperforms the numbers reported in [35] by 2.4%. We attribute the difference to variations in architectures and training schemes. Notably, this strong baseline, when using score fusion, reaches 53.1% average *mAP* (Table 3 row 4).

Transformer Network. Our next step is to simply replace the 1D convolutional network with our Transformer model using vanilla self-attention. This model achieves an average *mAP* of 58.7% (Table 3 row 5,) — a major boost of 15.9%. We note that this model already outperforms the best reported results (56.7% *mAP* at $tIoU=0.5$ from [45]). This result shows that our Transformer model is very powerful for TAL, and serves as the main course of performance gain.

Layer Norm, Center Sampling, Position Encoding, & Score Fusion. We further add layer norm in the classification and regression heads, apply center sampling during training, and explore position encoding as well as score fusion (Table 3 row 6-9). Adding layer norm boosts the average *mAP* by 2.7%, and using center sampling further improves the performance by 0.6%. The commonly used position encoding, however, decreased the average *mAP* slightly (-0.4%). We postulate that our projection using convolutions as well as the depthwise convolutions in our Transformer blocks already leak the location information, as also pointed out in [73]. Further fusing the classification scores produces another 1% boost. As a reference, when replacing the vanilla self-attention with a local version (window size=19), the average *mAP* remains the same.

Window Size for Local Self-Attention. Further, we study the effects of window size for local self-attention in our

Method	Win Size	0.5	0.7	Avg	GFLOPs
AF Base	N/A	55.0	33.1	53.1	45.6
Ours	9	65.7	42.6	62.5	45.2
Ours	19	65.6	42.7	62.6	45.3
Ours	25	65.8	42.0	62.4	45.4
Ours	37	65.7	42.8	62.5	45.5
Ours	Full	66.3	42.6	62.6	57.8

Table 4. **Ablation study on local window size in self-attention.** We report *mAP* at $tIoU=0.5$ and 0.7 , the average *mAP* in $[0.3 : 0.1 : 0.7]$ on THUMOS14, and the FLOPs by varying the local window size for self-attention in our model. FLOPs are reported on an input of 2304 time steps (about 5 minutes on THUMOS14).

Method	λ_{reg}	0.5	0.7	Avg
Ours	0.2	65.9	42.6	62.5
Ours	0.5	65.1	42.7	62.2
Ours	1	65.6	42.7	62.6
Ours	2	65.2	42.2	61.9
Ours	5	64.6	41.0	61.4

Table 5. **Ablation study on loss weight.** We report *mAP* at $tIoU=0.5$ and 0.7 , and the average *mAP* in $[0.3 : 0.1 : 0.7]$ on THUMOS14 by varying the loss weight λ_{reg} in Eq. 7.

Method	# Levels	Init Range	0.5	0.7	Avg
Ours	1	$[0, +\infty)$	49.2	18.7	45.5
Ours	3	$[0, 4)$	62.4	34.4	58.0
Ours	3	$[0, 8)$	60.2	34.5	56.1
Ours	3	$[0, 16)$	53.2	23.1	48.9
Ours	4	$[0, 4)$	63.8	38.4	60.1
Ours	5	$[0, 4)$	65.8	42.2	62.0
Ours	6	$[0, 4)$	65.6	42.7	62.6
Ours	7	$[0, 4)$	66.1	42.0	62.5

Table 6. **Ablation study on the design of feature pyramid.** We report *mAP* at $tIoU=0.5$ and 0.7 , and the average *mAP* in $[0.3 : 0.1 : 0.7]$ on THUMOS14 by varying (1) the number of pyramid levels and (2) the initial regression range

model. We vary the window size, re-train the model, and present both model accuracy and complexity (in GFLOPs) in Table 4. All results are reported with score fusion. Due to our design of a multiscale feature pyramid, even using the global self-attention only leads to 26% increase in FLOPs when compared to the baseline 1D convolutional network (see Table 3 row 4). Reducing the window size further cuts down the FLOPs yet maintains a similar accuracy.

For the rest of our ablation studies, we follow our best design and use a local window size=19 with layer norm, center sampling, and score fusion enabled.

Feature Pyramid. Moving forward, we study the design of the feature pyramid. As discussed in Sec. 3.3, our design space is specified by (1) the number of pyramid levels and (2) an initial regression range for the first level of the pyramid. We vary these parameters and report the results in Table 6.

First, we disable the feature pyramid and attach the classification and regression heads to the feature map with the highest resolution. This is done by setting the number of pyramid to 1 with an initial regression range of $[0, +\infty)$, Re-

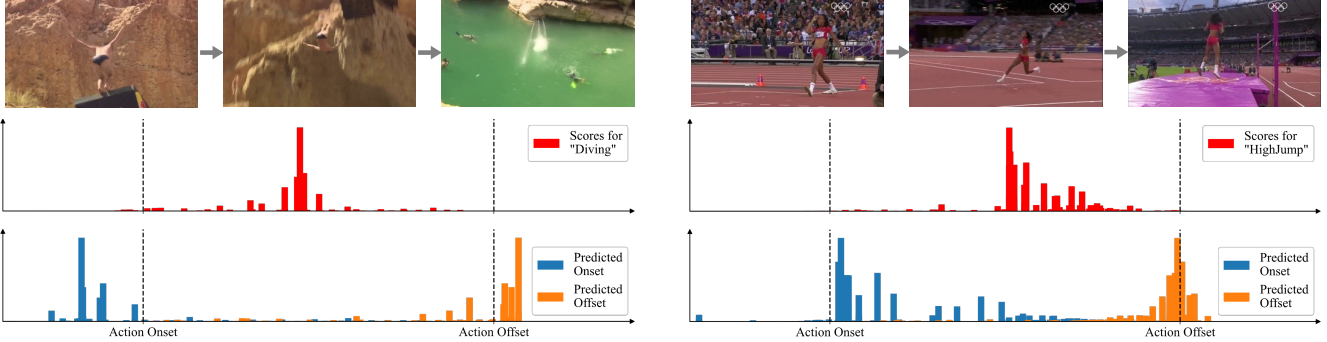


Figure 3. Visualization of our results. From *top* to *bottom*: (1) the input video frames; (2) action scores at each time step; (3) histogram of action onsets and offsets computed by weighting the regression outputs using the action scores. See more visualizations in the appendix.

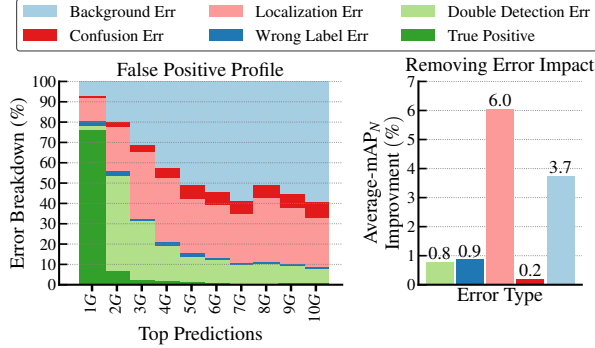


Figure 4. False positive (FP) profiling of our results on THUMOS14 using the tool from [1]. *Left*: FP error breakdown when considering the predictions for the top-10 ground-truth (G) instances. *Right*: The impact of error types. Our method suffers from background confusion and localization error.

moving the feature pyramid results in a major performance drop (-17.1% in average mAP), suggesting that using feature pyramid is critical for our model. Next, we set the number of pyramid levels to 3 and experiment with different initial regression ranges. The best results are achieved with the range of [0, 4). Further increase of the range decreases the mAP scores. Finally, we fix the initial regression range to [0, 4) and increase the number of pyramid levels. The performance of our method generally increases with more pyramid levels, yet is saturated when using 6 levels.

Loss Weight. We provide additional ablation on the loss weight λ_{reg} in Eq. 7. Specifically, we varied the loss weight $\lambda_{reg} \in [0.2, 0.5, 1, 2, 5]$, retrained the model, and reported the mAP scores. The results are presented in Table 5. For a large range of λ_{reg} , our model has quite stable results with a maximum gap of 1.5% in average mAP. $\lambda_{reg} = 1$ yields the best results, as we used in all our experiments.

Maximum Input Sequence Length during Training. A possible explanation of our superior results is that our model might benefit from training using a long sequence (2304 time steps as in our previous experiments). Here we examine the effects of maximum input sequence length during training. Table 7 reports mAP scores for different training sequence lengths. The results of our model remains fairly consistent

Method	T_{max}	0.5	0.7	Avg
Ours	576	65.8	41.5	62.2
Ours	1152	65.5	41.9	62.1
Ours	2304	65.6	42.7	62.6

Table 7. **Ablation study on maximum input sequence length during training.** We report mAP at tIoU=0.5 and 0.7, and the average mAP in [0.3 : 0.1 : 0.7] on THUMOS14 by varying the maximum input length T_{max} for training.

Method	stride	0.5	0.7	Avg
Ours	4	65.6	42.7	62.6
Ours	8	65.6	41.8	62.4
Ours	16	63.0	37.1	59.0

Table 8. **Ablation study on temporal feature resolution.** We report mAP at tIoU=0.5 and 0.7, and the average mAP in [0.3 : 0.1 : 0.7] on THUMOS14 by varying the feature stride.

even with much shorter input sequence length (*e.g.*, 576) similar to what was considered in [78]).

Temporal Feature Resolution. Some of the previous works considered video features with lower temporal resolution. For example, a feature stride of 8 was used by PGCN [80] and ContextLoc [88]. To understand the effects of temporal feature resolution, we downsample our input I3D features and study the performance variation when using different feature strides. Table 8 report the results. When using a lower resolution (stride=8), the results of our model only drop slightly (-0.2% in average mAP). Further reducing the resolution (*e.g.*, stride=16) leads to larger performance degradation, yet our results remains favourable.

Error Analysis. To better understand the error types, we provide additional analyses of our results. Specifically, we used the tool from [1] to analyze our results. The full analyses are included in the appendix. Here we highlight false positives profiling in Fig. 4. The two major types of error of our results are background confusion and localization error. Interestingly, the localization error has a higher impact to the final performance.

Result Visualization. Finally, we visualize the outputs of our model (before Soft-NMS) in Fig. 3, including the action scores, and the regression outputs weighted by the action

scores (as a weighted histogram). Our model outputs a strong peak near the center of an action, potentially due to the employment of center sampling during training. The regression of action boundaries seems less accurate. We conjecture that our regression heads can be further improved.

Why Does Our Model Work Well? Our comprehensive ablation experiments and analyses attempt to uncover the reason behind the superior results of our model. Based on our studies, the most important factor contributing to the performance is to use a Transformer backbone. Our model also benefits from the use of layer norm, center sampling, score fusion, and feature pyramid, while remaining relatively robust to the choice of local window size, loss weight, training sequence length, or feature resolution. It might be tempting to attribute the performance gain to the ability of modeling long-range dependencies using self-attention. However, our results on the local self-attention are against this argument. Indeed, our model achieves very competitive results even when using a small local window for self-attention (*e.g.* 9). Our conclusion is that our favourable performance is best explained by adapting the Transformer architecture into an orchestrated model design for temporal action localization.

5. Conclusion and Discussion

In this paper, we presented ActionFormer—a Transformer-based method for temporal action localization. ActionFormer has a simple design, falls into the category of single-stage anchor-free method, yet achieves impressive results across several major TAL benchmarks including THUMOS14, ActivityNet-1.3, and the more recent EPIC-Kitchens 100. Through our experiments, we showed that the power of ActionFormer lies in our design choices, in particular the combination of self-attention and a multiscale feature representation to model longer range temporal context in videos. We hope that our model, notwithstanding its simplicity, can shed light on the task of temporal action localization, and the more broader problem of video understanding.

Limitation. A main limitation of our method is the use of pre-extracted video features, also faced by many previous approaches. Another limitation is the need for many human labeled videos for training and the constraint of a pre-defined vocabulary of actions. Interesting future directions include pre-training for action localization [2, 75], and learning from videos and text corpus [30, 53] without human labels.

Appendix

This appendix provides further details of the main paper. We describe (1) implementation details and how to reproduce our results; (2) further error analysis of our results on THUMOS14; and (3) additional visualizations of our results.

A1. Implementation Details

We now present implementation details including the network architecture, training and inference. Further details can be found in our code.

Network Architecture. We present our network architecture in Table A.1, as described in Sec. 3.3. In the ablation study (Sec. 4.4), we also considered a baseline that replaces the Transformer Units in Table A.1 with convolution blocks, following the design of a bottleneck block in ResNet [27]. Specifically, a stack of three 1D conv layers were used. The kernel size of three conv layers were 1, 3 and 1, respectively. The expansion factor of the bottleneck block was 2. We added an extra strided conv layer with kernel size=1 and stride=2 to perform downsampling when necessary.

Training Details. For training, we considered both fixed length inputs (ActivityNet-1.3) and variable length inputs (THUMOS14, ActivityNet-1.3, and EPIC-Kitchens 100). For variable length inputs, we capped the input length to 2304 (around 5 minutes on THUMOS14 and around 20 minutes on EPIC-Kitchens 100), and randomly selected a subset of consecutive clips from an input video. Position embedding was disabled by default except for ActivityNet. Model EMA [28] and gradient clipping were also implemented to further stabilize the training. Hyperparameters were slightly different across datasets and listed in Sec. 4.1-4.3.

Inference Details. For fixed length inputs (ActivityNet-1.3), we fed the full sequence into our model. For variable length inputs (THUMOS14 and EPIC-Kitchens 100), we sent the full sequence into the model. When using position embeddings in our ablation study, we adopted the technique from [20]. Specifically, for input sequences shorter than the training sequence length (2304), we fed the full sequence into our model and clipped the position embedding using the actual length of the video. For input sequences longer than the training sequence length, we again fed the full sequence into our model, yet used linear interpolation to upsample the position embeddings.

Reproducibility of Our Results. We have included detailed instructions in our code to reproduce our best results on THUMOS14 (using I3D features from [41]), ActivityNet 1.3 (using TSP features from [2]), and EPIC Kitchens 100 (using SlowFast features from the model provided by [18]). All results reported in the paper were obtained with the same random seed using PyTorch 1.10, CUDA 10.2 and CUDNN 7.6.5 on an NVIDIA Titan Xp GPU, using deterministic GPU computing routines. On the same machine, our code

will always produce the same results when using the same random seed. Across machines/GPUs and computing environments, we have observed minor variation of average mAP scores (up to 0.5% average mAP on THUMOS, less than 0.2% average mAP on ActivityNet, and under 0.8% average mAP on EPIC Kitchens), yet those minor variations do not erode the clear performance gains of our method.

Further Error Analyses

We present further analyses of our results on THUMOS14, extending our Sec. 4.4 in the main paper. These analyses are obtained using the tool provided by [1]. We refer the readers to [1] for more details.

Metrics. In [1], several characteristic metrics were defined given a dataset (*e.g.* THUMOS14), including coverage, length, and the number of instances. Specifically, coverage presents the relative length of the actions (compared to the whole video), categorized into five bins: Extra Small (XS: (0, 0.02]), Small (S: (0.02, 0.04]), Medium (M: (0.04, 0.06]), Large (L: (0.06, 0.08]), and Extra Large (XL: (0.08, 1.0]). Length denotes the absolute length (in seconds) of actions, organized into five length groups: Extra Small (XS: (0, 3]), Small (S: (3, 6]), Medium (M: (6, 12]), Long (L: (12, 18]), and Extra Long (XL: > 18). Moreover, number of instances refers to the total count of instances (from the same class) in a video. This number is further divided into four parts, including Extra Small (XS: 1); Small (S: [2, 40]); Medium (M: [40, 80]); Large (L: > 80).

Results and Analyses. Fig. A.1 presents the false negative profiling. In Fig. A.1, we breakdown the false negative rates under the different coverage, length, and the number of instances. Our results have similar false negative rates across different coverage categories, yet have much higher false negative rates on action instances that are either very short or very long (length), and on videos that contain many action instances (#instances). These action instances and videos are naturally more challenging.

Fig. A.2 presents the sensitivity analysis of our results, *i.e.*, normalized mAP at tIoU=0.5 under different characteristic metrics (left) and the variance of mAP across categories (right). Our model performs better on simple context scenarios, including XS/S/M/L coverage, S/M length and XS #instances, and worse on more complicated scenarios. The trend is similar to the false negative profiling in Fig. A.1. Moreover, our model is robust across different categories in coverage, length and #instances with small variances.

Additional Visualizations

Further, we present more visualizations of our results in Fig. A.3, extending Fig. 3 of the main paper. Our model is able to detect the occurrence of actions and estimate their temporal boundaries for the most of the cases (see the first column of Fig. A.3). The major failure modes of our model,

as demonstrated in the second column of Fig. A.3, include (1) incorrect classification of action centers, *i.e.* background confusion (classification errors); (2) inaccurate regression of the action’s onset and offset (localization errors). We plan to address these issues in our future work.

References

- [1] Humam Alwassel, Fabian Caba Heilbron, Victor Escorcia, and Bernard Ghanem. Diagnosing error in temporal action detectors. In *Eur. Conf. Comput. Vis.*, volume 11207 of *LNCS*, pages 256–272, 2018. [9](#), [11](#), [12](#)
- [2] Humam Alwassel, Silvio Giancola, and Bernard Ghanem. TSP: Temporally-sensitive pretraining of video encoders for localization tasks. In *Int. Conf. Comput. Vis. Workshops*, pages 1–11, 2021. [6](#), [7](#), [10](#)
- [3] Anurag Arnab, Mostafa Dehghani, Georg Heigold, Chen Sun, Mario Lučić, and Cordelia Schmid. Vivit: A video vision transformer. In *Int. Conf. Comput. Vis.*, 2021. [2](#)
- [4] Yueran Bai, Yingying Wang, Yunhai Tong, Yang Yang, Qiyue Liu, and Junhui Liu. Boundary content graph neural network for temporal action proposal generation. In *Eur. Conf. Comput. Vis.*, volume 12373 of *LNCS*, pages 121–137, 2020. [1](#), [2](#), [6](#), [7](#)
- [5] Iz Beltagy, Matthew E. Peters, and Arman Cohan. Longformer: The long-document transformer. *arXiv:2004.05150*, 2020. [4](#)
- [6] Navaneeth Bodla, Bharat Singh, Rama Chellappa, and Larry S Davis. Soft-NMS—improving object detection with one line of code. In *Int. Conf. Comput. Vis.*, pages 5561–5569, 2017. [5](#)
- [7] Shyamal Buch, Victor Escorcia, Bernard Ghanem, and Juan Niebles Carlos. End-to-end, single-stream temporal action detection in untrimmed videos. In *Brit. Mach. Vis. Conf.*, pages 93.1–93.12, 2017. [1](#), [2](#)
- [8] Shyamal Buch, Victor Escorcia, Chuanqi Shen, Bernard Ghanem, and Juan Carlos Niebles. SST: Single-stream temporal action proposals. In *IEEE Conf. Comput. Vis. Pattern Recog.*, pages 2911–2920, 2017. [2](#)
- [9] Fabian Caba Heilbron, Juan Carlos Niebles, and Bernard Ghanem. Fast temporal activity proposals for efficient detection of human actions in untrimmed videos. In *IEEE Conf. Comput. Vis. Pattern Recog.*, pages 1914–1923, 2016. [2](#)
- [10] Fabian Caba Heilbron, Victor Escorcia, Bernard Ghanem, and Juan Carlos Niebles. ActivityNet: A large-scale video benchmark for human activity understanding. In *IEEE Conf. Comput. Vis. Pattern Recog.*, pages 961–970, 2015. [5](#), [7](#)

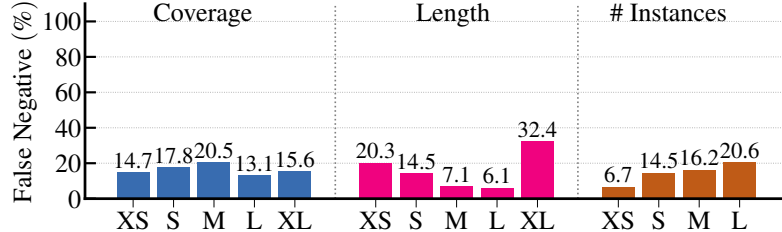


Figure A.1. False negative (FN) profiling of our results on THUMOS14 using [1]. This figure shows the FN rates under different video contents. From this figure we can find that our model will suffer from extra short or extra long instances. Also, our model will suffer from video inputs which have a large number of action instances.

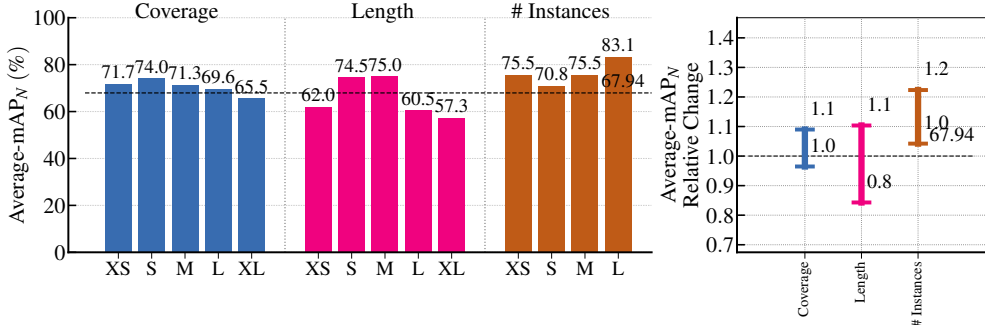


Figure A.2. Sensitive analysis of our results on THUMOS14 using [1]. Left: normalized mAP at $tIoU=0.5$ under different video contents. Right: The relative normalized mAP change at $tIoU=0.5$ with respect to different characteristics of the ground truth instances.

	Name	Layer	Input	Output Size ($T \times D$)	Regression Range
encoder	input clip	-	-	$T \times D$	-
	projection1	conv $k=3, s=1 (c_i = D, c_o = 512)$	input clip	$T \times 512$	-
	projection2	conv $k=3, s=1 (c_i = 512, c_o = 512)$	projection1	$T \times 512$	-
	transformer0	Transformer Unit, $ds=1$	projection2	$T \times 512$	-
	transformer1	Transformer Unit, $ds=1$	transformer0	$T \times 512$	[0, 4)
	transformer2	Transformer Unit, $ds=2$	transformer1	$T/2 \times 512$	[4, 8)
	transformer3	Transformer Unit, $ds=2$	transformer2	$T/4 \times 512$	[8, 16)
	transformer4	Transformer Unit, $ds=2$	transformer3	$T/8 \times 512$	[16, 32)
	transformer5	Transformer Unit, $ds=2$	transformer4	$T/16 \times 512$	[32, 64)
	transformer6	Transformer Unit, $ds=2$	transformer5	$T/32 \times 512$	[64, ∞)
decoder (heads)	cls / reg nets	conv $k=3, s=1 (c_i = 512, c_o = 512)$ conv $k=3, s=1 (c_i = 512, c_o = 512)$ conv $k=3, s=1 (c_i = 512, c_o = \text{output})$	transformer1,...,transformer6 transformer1,...,transformer6 transformer1,...,transformer6	[$T/32 \times 512, \dots, T \times 512$] [$T/32 \times 512, \dots, T \times 512$] [$T/32 \times \text{output}, \dots, T \times \text{output}$]	- - -

Table A.1. **The architecture of our model.** Our network consists of (1) a Transformer encoder (first row block) and (2) a lightweight convolutional decoder with the classification / regression heads (last row block). For each layer, we list the layer name, layer parameters, the input to the layer, and the output feature size. We also include its regression range (in seconds for THUMOS14 and EPIC-Kitchens 100 and in number of time steps for ActivityNet-1.3). For convolutional layers, k is the kernel size of 1D convolutions and s is the stride, and c_i, c_o is the input and output feature channel, respectively. For Transformer Unit, ds is the downsampling ratio. T is the temporal length of input sequence and D is the input feature dimension. For classification head, the output dimension is the number of action categories. For regression head, the output dimension is 2, *i.e.*, distances to action onset and offset.

- [11] Nicolas Carion, Francisco Massa, Gabriel Synnaeve, Nicolas Usunier, Alexander Kirillov, and Sergey Zagoruyko. End-to-end object detection with transformers. In *Eur. Conf. Comput. Vis.*, volume 12346 of *LNCS*, pages 213–229, 2020. [1](#) [2](#)
- [12] Joao Carreira and Andrew Zisserman. Quo vadis, action recognition? a new model and the Kinetics dataset. In *IEEE Conf. Comput. Vis. Pattern Recog.*, pages 4724–4733, 2017. [6](#) [7](#)
- [13] Shuning Chang, Pichao Wang, Fan Wang, Hao Li, and Jiashi Feng. Augmented transformer with adaptive graph for temporal action proposal generation. *arXiv preprint arXiv:2103.16024*, 2021. [2](#)
- [14] Yu-Wei Chao, Sudheendra Vijayanarasimhan, Bryan Seybold, David A Ross, Jia Deng, and Rahul Sukthankar. Rethinking the Faster-RCNN architecture for temporal action localization. In *IEEE Conf. Comput. Vis. Pattern Recog.*, pages 1130–1139, 2018. [2](#) [6](#)
- [15] Bowen Cheng, Alexander G Schwing, and Alexander Kirillov. Per-pixel classification is not all you need for

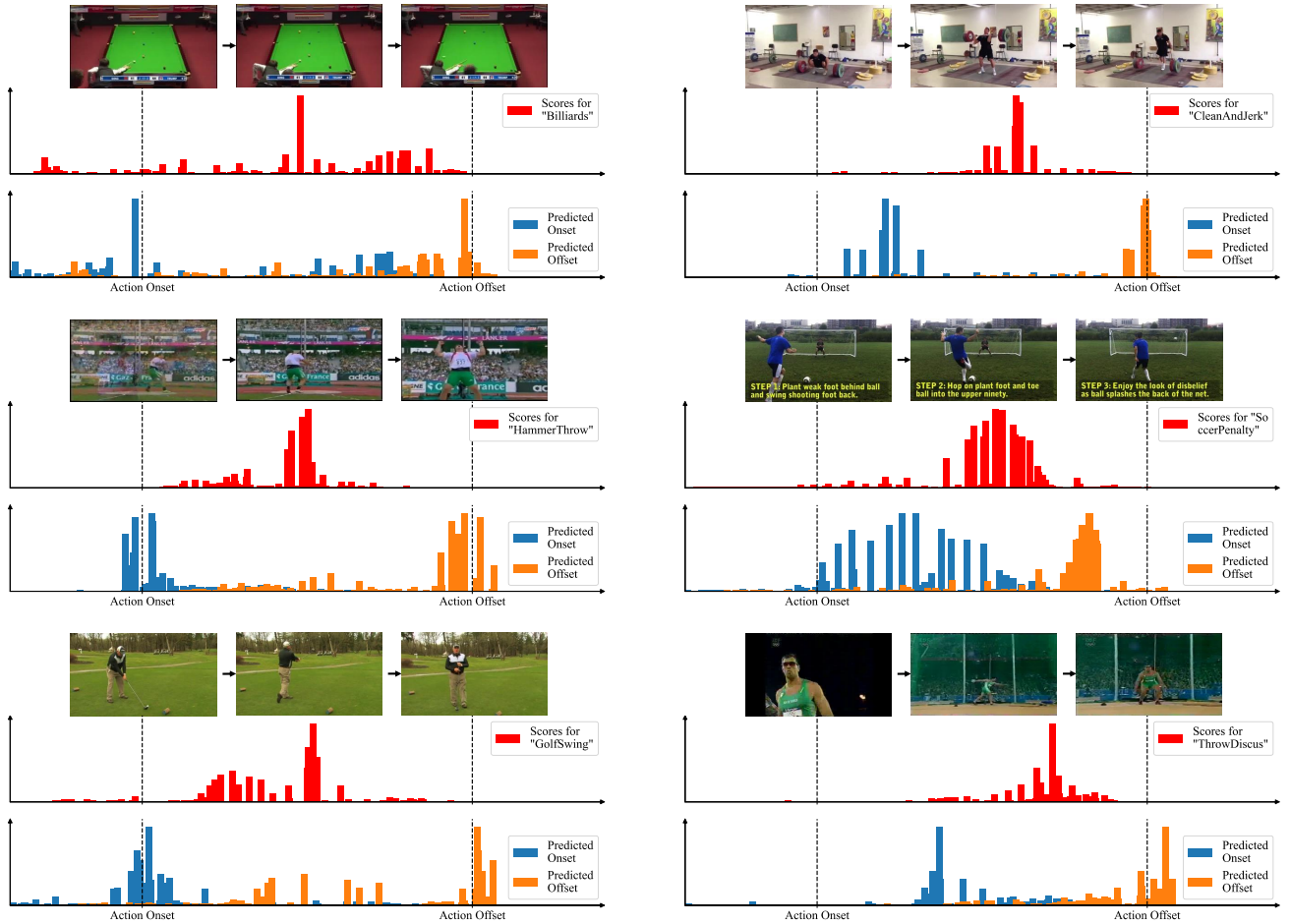


Figure A.3. More visualization of our outputs. Visualization of our results. From *top* to *bottom*: (1) the input video frames; (2) action scores at each time step; (3) histogram of action onsets and offsets computed by weighting the regression outputs using the action scores. *Left*: successful cases; *Right*: failure cases. This figure is best viewed in color and when zoomed in.

semantic segmentation. In *Adv. Neural Inform. Process. Syst.*, 2021. 2

[16] Krzysztof Choromanski, Valerii Likhoshesterov, David Dohan, Xingyou Song, Andreea Gane, Tamas Sarlos, Peter Hawkins, Jared Davis, Afroz Mohiuddin, Lukasz Kaiser, et al. Rethinking attention with performers. *Int. Conf. Learn. Represent.*, 2021. 4

[17] Xiyang Dai, Yinpeng Chen, Jianwei Yang, Pengchuan Zhang, Lu Yuan, and Lei Zhang. Dynamic DETR: End-to-end object detection with dynamic attention. In *Int. Conf. Comput. Vis.*, pages 2988–2997, 2021. 2

[18] Dima Damen, Hazel Doughty, Giovanni Maria Farinella, Antonino Furnari, Evangelos Kazakos, Jian Ma, Davide Moltisanti, Jonathan Munro, Toby Perrett, Will Price, et al. Rescaling egocentric vision. *arXiv preprint arXiv:2006.13256*, 2020. 5, 7, 10

[19] Jacob Devlin, Ming-Wei Chang, Kenton Lee, and Kristina Toutanova. BERT: Pre-training of deep bidi-

rectional transformers for language understanding. In *North American Asso. Comput. Lin.*, pages 4171–4186, 2019. 1

[20] Alexey Dosovitskiy, Lucas Beyer, Alexander Kolesnikov, Dirk Weissenborn, Xiaohua Zhai, Thomas Unterthiner, Mostafa Dehghani, Matthias Minderer, Georg Heigold, Sylvain Gelly, et al. An image is worth 16x16 words: Transformers for image recognition at scale. In *Int. Conf. Learn. Represent.*, 2021. 1, 2, 10

[21] Kaiwen Duan, Song Bai, Lingxi Xie, Honggang Qi, Qingming Huang, and Qi Tian. CenterNet: Keypoint triplets for object detection. In *Int. Conf. Comput. Vis.*, pages 6569–6578, 2019. 2

[22] Victor Escorcia, Fabian Caba Heilbron, Juan Carlos Niebles, and Bernard Ghanem. DAPs: Deep action proposals for action understanding. In *Eur. Conf. Comput. Vis.*, volume 9907 of *LNCS*, pages 768–784, 2016. 2

[23] Haoqi Fan, Bo Xiong, Karttikeya Mangalam, Yang-hao Li, Zhicheng Yan, Jitendra Malik, and Christoph Feichtenhofer. Multiscale vision transformers. *arXiv preprint arXiv:2104.11227*, 2021. [2](#)

[24] Christoph Feichtenhofer, Haoqi Fan, Jitendra Malik, and Kaiming He. SlowFast networks for video recognition. In *Int. Conf. Comput. Vis.*, pages 6202–6211, 2019. [6](#), [7](#)

[25] Rohit Girdhar, Joao Carreira, Carl Doersch, and Andrew Zisserman. Video action transformer network. In *IEEE Conf. Comput. Vis. Pattern Recog.*, pages 244–253, 2019. [2](#), [5](#)

[26] Guoqiang Gong, Liangfeng Zheng, and Yadong Mu. Scale matters: Temporal scale aggregation network for precise action localization in untrimmed videos. In *Int. Conf. Multimedia and Expo*, pages 1–6. IEEE, 2020. [2](#), [6](#)

[27] Kaiming He, Xiangyu Zhang, Shaoqing Ren, and Jian Sun. Deep residual learning for image recognition. In *IEEE Conf. Comput. Vis. Pattern Recog.*, pages 770–778, 2016. [10](#)

[28] Gao Huang, Yixuan Li, Geoff Pleiss, Zhuang Liu, John E Hopcroft, and Kilian Q Weinberger. Snapshot ensembles: Train 1, get m for free. In *Int. Conf. Learn. Represent.*, 2017. [10](#)

[29] Haroon Idrees, Amir R Zamir, Yu-Gang Jiang, Alex Gorban, Ivan Laptev, Rahul Sukthankar, and Mubarak Shah. The THUMOS challenge on action recognition for videos “in the wild”. *Comput. Vis. and Image Under.*, 155:1–23, 2017. [5](#)

[30] Chao Jia, Yinfai Yang, Ye Xia, Yi-Ting Chen, Zarana Parekh, Hieu Pham, Quoc V Le, Yunhsuan Sung, Zhen Li, and Tom Duerig. Scaling up visual and vision-language representation learning with noisy text supervision. In *Int. Conf. Mach. Learn.*, 2021. [10](#)

[31] Diederik P Kingma and Jimmy Ba. Adam: A method for stochastic optimization. In *Int. Conf. Learn. Represent.*, pages 1–11, 2015. [5](#)

[32] Shiyang Li, Xiaoyong Jin, Yao Xuan, Xiyu Zhou, Wenhui Chen, Yu-Xiang Wang, and Xifeng Yan. Enhancing the locality and breaking the memory bottleneck of transformer on time series forecasting. In *Adv. Neural Inform. Process. Syst.*, volume 32, 2019. [4](#)

[33] Xin Li, Tianwei Lin, Xiao Liu, Wangmeng Zuo, Chao Li, Xiang Long, Dongliang He, Fu Li, Shilei Wen, and Chuang Gan. Deep concept-wise temporal convolutional networks for action localization. In *Proceedings of the 28th ACM International Conference on Multimedia*, pages 4004–4012, 2020. [6](#), [7](#)

[34] Chuming Lin, Jian Li, Yabiao Wang, Ying Tai, Dong-hao Luo, Zhipeng Cui, Chengjie Wang, Jilin Li, Feiyue Huang, and Rongrong Ji. Fast learning of temporal action proposal via dense boundary generator. In *AAAI*, pages 11499–11506, 2020. [6](#)

[35] Chuming Lin, Chengming Xu, Donghao Luo, Yabiao Wang, Ying Tai, Chengjie Wang, Jilin Li, Feiyue Huang, and Yanwei Fu. Learning salient boundary feature for anchor-free temporal action localization. In *IEEE Conf. Comput. Vis. Pattern Recog.*, pages 3320–3329, 2021. [2](#), [3](#), [6](#), [8](#)

[36] Tianwei Lin, Xiao Liu, Xin Li, Errui Ding, and Shilei Wen. BMN: Boundary-matching network for temporal action proposal generation. In *Int. Conf. Comput. Vis.*, pages 3889–3898, 2019. [1](#), [2](#), [6](#), [7](#)

[37] Tianwei Lin, Xu Zhao, and Zheng Shou. Single shot temporal action detection. In *ACM Int. Conf. Multimedia*, pages 988–996, 2017. [2](#)

[38] Tianwei Lin, Xu Zhao, Haisheng Su, Chongjing Wang, and Ming Yang. BSN: Boundary sensitive network for temporal action proposal generation. In *Eur. Conf. Comput. Vis.*, volume 11208 of *LNCS*, pages 3–19, 2018. [2](#), [6](#), [7](#)

[39] Tsung-Yi Lin, Piotr Dollár, Ross Girshick, Kaiming He, Bharath Hariharan, and Serge Belongie. Feature pyramid networks for object detection. In *IEEE Conf. Comput. Vis. Pattern Recog.*, pages 2117–2125, 2017. [2](#), [5](#)

[40] Tsung-Yi Lin, Priya Goyal, Ross Girshick, Kaiming He, and Piotr Dollár. Focal loss for dense object detection. In *Int. Conf. Comput. Vis.*, pages 2980–2988, 2017. [2](#), [5](#)

[41] Daochang Liu, Tingting Jiang, and Yizhou Wang. Completeness modeling and context separation for weakly supervised temporal action localization. In *IEEE Conf. Comput. Vis. Pattern Recog.*, pages 1298–1307, 2019. [6](#), [10](#)

[42] Liyuan Liu, Xiaodong Liu, Jianfeng Gao, Weizhu Chen, and Jiawei Han. Understanding the difficulty of training transformers. In *Proceedings of the 2020 Conference on Empirical Methods in Natural Language Processing (EMNLP)*, pages 5747–5763, 2020. [5](#)

[43] Qinying Liu and Zilei Wang. Progressive boundary refinement network for temporal action detection. In *AAAI*, volume 34, pages 11612–11619, 2020. [6](#)

[44] Wei Liu, Dragomir Anguelov, Dumitru Erhan, Christian Szegedy, Scott Reed, Cheng-Yang Fu, and Alexander C Berg. SSD: Single shot multibox detector. In *Eur. Conf. Comput. Vis.*, pages 21–37, 2016. [2](#)

[45] Xiaolong Liu, Yao Hu, Song Bai, Fei Ding, Xiang Bai, and Philip HS Torr. Multi-shot temporal event localization: a benchmark. In *IEEE Conf. Comput. Vis. Pattern Recog.*, pages 12596–12606, 2021. [6](#), [8](#)

[46] Xiaolong Liu, Qimeng Wang, Yao Hu, Xu Tang, Song Bai, and Xiang Bai. End-to-end temporal action detection with transformer. *arXiv preprint arXiv:2106.10271*, 2021. [2](#), [6](#), [7](#)

[47] Yuan Liu, Lin Ma, Yifeng Zhang, Wei Liu, and Shih-Fu Chang. Multi-granularity generator for temporal action proposal. In *IEEE Conf. Comput. Vis. Pattern Recog.*, pages 3604–3613, 2019. [2](#)

[48] Ze Liu, Yutong Lin, Yue Cao, Han Hu, Yixuan Wei, Zheng Zhang, Stephen Lin, and Baining Guo. Swin transformer: Hierarchical vision transformer using shifted windows. In *Int. Conf. Comput. Vis.*, 2021. [1](#), [2](#)

[49] Ze Liu, Jia Ning, Yue Cao, Yixuan Wei, Zheng Zhang, Stephen Lin, and Han Hu. Video swin transformer. *arXiv preprint arXiv:2106.13230*, 2021. [2](#)

[50] Fuchen Long, Ting Yao, Zhaofan Qiu, Xinmei Tian, Jiebo Luo, and Tao Mei. Gaussian temporal awareness networks for action localization. In *IEEE Conf. Comput. Vis. Pattern Recog.*, pages 344–353, 2019. [1](#), [2](#), [6](#)

[51] Zhiwu Qing, Haisheng Su, Weihao Gan, Dongliang Wang, Wei Wu, Xiang Wang, Yu Qiao, Junjie Yan, Changxin Gao, and Nong Sang. Temporal context aggregation network for temporal action proposal refinement. In *IEEE Conf. Comput. Vis. Pattern Recog.*, pages 485–494, 2021. [2](#), [6](#), [7](#)

[52] Zhaofan Qiu, Ting Yao, and Tao Mei. Learning spatio-temporal representation with pseudo-3d residual networks. In *Int. Conf. Comput. Vis.*, pages 5533–5541, 2017. [6](#)

[53] Alec Radford, Jong Wook Kim, Chris Hallacy, Aditya Ramesh, Gabriel Goh, Sandhini Agarwal, Girish Sastry, Amanda Askell, Pamela Mishkin, Jack Clark, et al. Learning transferable visual models from natural language supervision. In *Int. Conf. Mach. Learn.*, 2021. [10](#)

[54] Hamid Rezatofighi, Nathan Tsoi, JunYoung Gwak, Amir Sadeghian, Ian Reid, and Silvio Savarese. Generalized intersection over union: A metric and a loss for bounding box regression. In *IEEE Conf. Comput. Vis. Pattern Recog.*, pages 658–666, 2019. [5](#)

[55] Zheng Shou, Jonathan Chan, Alireza Zareian, Kazuyuki Miyazawa, and Shih-Fu Chang. CDC: Convolutional-de-convolutional networks for precise temporal action localization in untrimmed videos. In *IEEE Conf. Comput. Vis. Pattern Recog.*, pages 5734–5743, 2017. [1](#), [2](#), [6](#)

[56] Zheng Shou, Dongang Wang, and Shih-Fu Chang. Temporal action localization in untrimmed videos via multi-stage CNNs. In *IEEE Conf. Comput. Vis. Pattern Recog.*, pages 1049–1058, 2016. [2](#)

[57] Karen Simonyan and Andrew Zisserman. Two-stream convolutional networks for action recognition in videos. In *Adv. Neural Inform. Process. Syst.*, pages 568–576, 2014. [6](#)

[58] Deepak Sridhar, Niamul Quader, Srikanth Muralidharan, Yaxin Li, Peng Dai, and Juwei Lu. Class semantics-based attention for action detection. In *Int. Conf. Comput. Vis.*, pages 13739–13748, 2021. [2](#), [6](#), [7](#)

[59] Jing Tan, Jiaqi Tang, Limin Wang, and Gangshan Wu. Relaxed transformer decoders for direct action proposal generation. In *Int. Conf. Comput. Vis.*, pages 13526–13535, 2021. [2](#), [6](#)

[60] Zhi Tian, Chunhua Shen, Hao Chen, and Tong He. FCOS: Fully convolutional one-stage object detection. In *Int. Conf. Comput. Vis.*, pages 9627–9636, 2019. [2](#), [5](#)

[61] Hugo Touvron, Matthieu Cord, Matthijs Douze, Francisco Massa, Alexandre Sablayrolles, and Hervé Jégou. Training data-efficient image transformers & distillation through attention. In *Int. Conf. Mach. Learn.*, pages 10347–10357, 2021. [2](#)

[62] Hugo Touvron, Matthieu Cord, Alexandre Sablayrolles, Gabriel Synnaeve, and Hervé Jégou. Going deeper with image transformers. In *Int. Conf. Comput. Vis.*, 2021. [4](#)

[63] Du Tran, Heng Wang, Lorenzo Torresani, Jamie Ray, Yann LeCun, and Manohar Paluri. A closer look at spatiotemporal convolutions for action recognition. In *IEEE Conf. Comput. Vis. Pattern Recog.*, pages 6450–6459, 2018. [6](#)

[64] Ashish Vaswani, Noam Shazeer, Niki Parmar, Jakob Uszkoreit, Llion Jones, Aidan N Gomez, Łukasz Kaiser, and Illia Polosukhin. Attention is all you need. In *Adv. Neural Inform. Process. Syst.*, pages 5998–6008, 2017. [1](#), [2](#), [3](#), [4](#)

[65] Limin Wang, Yuanjun Xiong, Dahua Lin, and Luc Van Gool. UntrimmedNets for weakly supervised action recognition and detection. In *IEEE Conf. Comput. Vis. Pattern Recog.*, pages 4325–4334, 2017. [6](#)

[66] Limin Wang, Yuanjun Xiong, Zhe Wang, Yu Qiao, Dahua Lin, Xiaou Tang, and Luc Van Gool. Temporal segment networks: Towards good practices for deep action recognition. In *Eur. Conf. Comput. Vis.*, volume 11205 of *LNCS*, pages 20–36, 2016. [6](#)

[67] Lining Wang, Haosen Yang, Wenhao Wu, Hongxun Yao, and Hujie Huang. Temporal action proposal generation with transformers. *arXiv preprint arXiv:2105.12043*, 2021. [2](#)

[68] Sinong Wang, Belinda Li, Madian Khabsa, Han Fang, and Hao Ma. Linformer: Self-attention with linear complexity. *arXiv preprint arXiv:2006.04768*, 2020. 4

[69] Tao Wang, Li Yuan, Yunpeng Chen, Jiashi Feng, and Shuicheng Yan. PnP-DETR: Towards efficient visual analysis with transformers. In *Int. Conf. Comput. Vis.*, pages 4661–4670, 2021. 2

[70] Wenhai Wang, Enze Xie, Xiang Li, Deng-Ping Fan, Kaitao Song, Ding Liang, Tong Lu, Ping Luo, and Ling Shao. Pyramid vision transformer: A versatile backbone for dense prediction without convolutions. In *Int. Conf. Comput. Vis.*, 2021. 2

[71] Yuqing Wang, Zhaoliang Xu, Xinlong Wang, Chunhua Shen, Baoshan Cheng, Hao Shen, and Huaxia Xia. End-to-end video instance segmentation with Transformers. In *IEEE Conf. Comput. Vis. Pattern Recog.*, pages 8741–8750, 2021. 2

[72] Tete Xiao, Mannat Singh, Eric Mintun, Trevor Darrell, Piotr Dollár, and Ross Girshick. Early convolutions help transformers see better. In *Adv. Neural Inform. Process. Syst.*, 2021. 4

[73] Enze Xie, Wenhai Wang, Zhiding Yu, Anima Anandkumar, Jose M Alvarez, and Ping Luo. Segformer: Simple and efficient design for semantic segmentation with transformers. In *Adv. Neural Inform. Process. Syst.*, 2021. 2, 8

[74] Yunyang Xiong, Zhanpeng Zeng, Rudrasis Chakraborty, Mingxing Tan, Glenn Fung, Yin Li, and Vikas Singh. Nyströmformer: A nyström-based algorithm for approximating self-attention. In *AAAI*, volume 35, pages 14138–14148, 2021. 4

[75] Mengmeng Xu, Juan-Manuel Pérez-Rúa, Victor Escorcia, Brais Martínez, Xiatian Zhu, Li Zhang, Bernard Ghanem, and Tao Xiang. Boundary-sensitive pre-training for temporal localization in videos. In *Int. Conf. Comput. Vis.*, pages 7220–7230, 2021. 10

[76] Mengmeng Xu, Chen Zhao, David S Rojas, Ali Thabet, and Bernard Ghanem. G-TAD: Sub-graph localization for temporal action detection. In *IEEE Conf. Comput. Vis. Pattern Recog.*, pages 10156–10165, 2020. 1, 2, 6, 7

[77] Jianwei Yang, Chunyuan Li, Pengchuan Zhang, Xiyang Dai, Bin Xiao, Lu Yuan, and Jianfeng Gao. Focal self-attention for local-global interactions in vision transformers. In *Adv. Neural Inform. Process. Syst.*, 2021. 2

[78] Le Yang, Houwen Peng, Dingwen Zhang, Jianlong Fu, and Junwei Han. Revisiting anchor mechanisms for temporal action localization. *IEEE Trans. Image Process.*, 29:8535–8548, 2020. 2, 3, 5, 6, 8, 9

[79] Li Yuan, Yunpeng Chen, Tao Wang, Weihao Yu, Yujun Shi, Zihang Jiang, Francis EH Tay, Jiashi Feng, and Shuicheng Yan. Tokens-to-token ViT: Training vision transformers from scratch on ImageNet. In *Int. Conf. Comput. Vis.*, 2021. 2

[80] Runhao Zeng, Wenbing Huang, Mingkui Tan, Yu Rong, Peilin Zhao, Junzhou Huang, and Chuang Gan. Graph convolutional networks for temporal action localization. In *Int. Conf. Comput. Vis.*, pages 7094–7103, 2019. 2, 6, 7, 9

[81] Runhao Zeng, Haoming Xu, Wenbing Huang, Peihao Chen, Mingkui Tan, and Chuang Gan. Dense regression network for video grounding. In *IEEE Conf. Comput. Vis. Pattern Recog.*, pages 10287–10296, 2020. 2

[82] Shifeng Zhang, Cheng Chi, Yongqiang Yao, Zhen Lei, and Stan Z Li. Bridging the gap between anchor-based and anchor-free detection via adaptive training sample selection. In *IEEE Conf. Comput. Vis. Pattern Recog.*, pages 9759–9768, 2020. 2, 5

[83] Chen Zhao, Ali K Thabet, and Bernard Ghanem. Video self-stitching graph network for temporal action localization. In *Int. Conf. Comput. Vis.*, pages 13658–13667, 2021. 2, 6, 7

[84] Peisen Zhao, Lingxi Xie, Chen Ju, Ya Zhang, Yanfeng Wang, and Qi Tian. Bottom-up temporal action localization with mutual regularization. In *Eur. Conf. Comput. Vis.*, volume 12353 of *LNCS*, pages 539–555, 2020. 2, 6, 7

[85] Yue Zhao, Yuanjun Xiong, Limin Wang, Zhirong Wu, Xiaoou Tang, and Dahua Lin. Temporal action detection with structured segment networks. In *Int. Conf. Comput. Vis.*, pages 2914–2923, 2017. 1, 2, 6

[86] Yue Zhao, Bo wen Zhang, Zhirong Wu, Shuo Yang, Lei Zhou, Sijie Yan, Limin Wang, Yuanjun Xiong, Dahua Lin, Yu Qiao, and Xiaoou Tang. CUHK & ETHZ & SIAT submission to ActivityNet challenge 2017. *arXiv preprint arXiv:1710.08011*, 2017. 7

[87] Xizhou Zhu, Weijie Su, Lewei Lu, Bin Li, Xiaogang Wang, and Jifeng Dai. Deformable detr: Deformable transformers for end-to-end object detection. In *Int. Conf. Learn. Represent.*, pages 1–11, 2021. 2

[88] Zixin Zhu, Wei Tang, Le Wang, Nanning Zheng, and Gang Hua. Enriching local and global contexts for temporal action localization. In *Int. Conf. Comput. Vis.*, pages 13516–13525, 2021. 2, 6, 9